Nanoscale

RSC Publishing

PAPER

View Article Online
View Journal | View Issue

Cite this: *Nanoscale*, 2013, **5**, 5958

A high performance hybrid capacitor with Li_2CoPO_4F cathode and activated carbon anode†

K. Karthikeyan,[a] S. Amaresh,[a] K. J. Kim,[a] S. H. Kim,[a] K. Y. Chung,[b] B. W. Cho[b] and Y. S. Lee*[a]

Received 12th February 2013
Accepted 17th April 2013

DOI: 10.1039/c3nr00760j

www.rsc.org/nanoscale

For the first time, we report the possibility of utilizing Li_2CoPO_4F as a novel cathode material for hybrid capacitor applications. Li_2CoPO_4F powders were prepared by a conventional two-step solid state method. A hybrid cell was fabricated using Li_2CoPO_4F as the cathode along with activated carbon (AC) as the anode in 1 M $LiPF_6$ dissolved in 1 : 1 EC/DMC electrolyte and its electrochemical properties were examined by cyclic voltammetry (CV), electrochemical impedance spectroscopy (EIS) and constant current charge–discharge (C–D) techniques. The Li_2CoPO_4F/AC cell is capable of delivering a discharge capacitance of 42 F g^{-1} at 150 mA g^{-1} current density within 0–3 V region having excellent coulombic efficiency of over 99% even after 1000 cycles. Furthermore, the Li_2CoPO_4F/AC cell exhibited excellent rate performance with an energy density of ~24 W h kg^{-1} at 1100 mA g^{-1} current and maintained about 92% of its initial value even after 30 000 C–D cycles. Electrochemical impedance spectroscopy was conducted to corroborate the results that were obtained and described.

1 Introduction

In recent times, new energy devices with high energy and power densities have been focused by increasing research groups due to the environmental concerns and depleting fossil fuels. It is well known that supercapacitors (SCs) or ultracapacitors are promising devices for energy storage because their characteristics are located between those of dielectric capacitors and those of conventional batteries. High specific power, a long cycle life at high rate over short time, small and light weight package, and application simplicity of SCs expand their usage to various integrated power applications.[1] In general, supercapacitors are classified into two main categories based on the storage mechanism utilized, namely, electric double-layer capacitors (EDLCs) and pseudo-capacitors. EDLCs with various types of carbon based materials have been used as electrodes in order to utilize the double-layer capacitance.[2] On the other hand, pseudo-capacitors with transition metal oxides or conducting polymers have been used as electrodes in order to utilize the charge-transfer pseudo-capacitance.[3,4] EDLCs offer a high power density, a good reversibility and a long cycle life. Pseudo-capacitors have a much higher energy density and a lower cycle life than EDLCs. Hybridization of two types of electrodes to form a new capacitor called a hybrid supercapacitor (HSC) is a unique approach that is used to enhance the electrochemical properties of a single cell. HSCs exhibit electrochemical behavior over different voltage ranges, which enhances the overall operating voltage window and their specific energy density becomes larger than the cells containing sole kind of electrode.[5–8] In this case, one of the electrodes is an energy source electrode (battery like electrodes) and the other terminal contains a power source electrode (either an EDLC or a pseudo capacitor electrode). The choice of the energy source electrode is also important because this electrode enhances the cell voltage without sacrificing the energy and power densities. The HSC fabricated with an EDLC type electrode and a battery type (especially intercalating materials) electrode offers the advantages of both supercapacitors and the advanced batteries, which results in a significant increase in the overall energy density of the system compared with that of the AC/AC system.[5,9]

Recently, various lithium intercalation compounds have been adopted as electrode materials for HSCs.[10–15] As the aforementioned energy source electrodes, the Mn based materials have attracted immense attention because they are environmentally benign and cost effective with higher operating voltages. Spinel $LiMn_2O_4$ has been extensively studied as an electrode material for hybrid supercapacitors. However, capacity fading is encountered in the 3 V regions during prolonged cycling due to Jahn–Teller distortion that is associated with the average valence of manganese, which falls below +3.5 in $LiMn_2O_4$. To overcome these issues, various metal ions, such as $LiM_xMn_{2-x}O_4$ (M = Ni, Cr, and Co), have been used as substitutes and these new materials have been investigated as

[a]*Faculty of Applied Chemical Engineering, Chonnam National University, Gwangju 500-757, Korea. E-mail: leeys@chonnam.ac.kr; Fax: +82 62 530 1904; Tel: +82 62 530 1904*

[b]*Center for Energy Convergence, Korea Institute of Science and Technology, Seoul 136-791, Korea*

† Electronic supplementary information (ESI) available. See DOI: 10.1039/c3nr00760j

cathodes for hybrid electrochemical devices.[16] Nevertheless, the capacity fading has been minimized but not effectively prevented. Furthermore, a new class of fluoro-oxyanions with a general formula of A_2MPO_4F (A = Li, Na and M = Fe, Mn, Co, Ni) is being developed as high-voltage cathode materials for advanced lithium ion batteries application.[17–20] Among them, Li_2CoPO_4F (LCPF) is considered as the promising candidate because of its high theoretical capacity and high redox potential, which make it an attractive candidate for cathodes used in high-energy batteries. However, till now, very limited reports have been made on the preparation and electrochemical characteristics of LCPF for LIB application.[21,24]

In our previous studies, we succeeded in demonstrating a HSC based on poly anion type lithium insertion hosts Li_2MSiO_4 (M = Mn or Fe) and AC with excellent cycleability.[25,26] Cathode materials based on fluorophosphates (LCPF) can also be considered as high energy source materials for HSC applications. The structure of LCPF possesses a 3D framework, in which corner-shared CoO_6 and edge-shared CoO_4F_2 octahedra are interconnected by PO_4 tetrahedra with channels occupied by Li ions.[21] This 3D framework structure is expected to allow the diffusion of Li ions through its extended channels along with [010] and [011] directions.[20,21,24] In addition, the presence of highly electronegative F^- ions in the crystal structure provided much more stability than their counterpart oxygen ions.[17,19] Because, the M–F bonds have higher ionicity than M–O bonds and hence it was expected to enhance the potential of the corresponding $M^{n/n+1}$ redox couple than phosphates.[23,24] However, extensive studies are required for adopting the LCPF material as a potential cathode material for lithium-ion batteries in practical use. Although LCPF did not show stable electrochemical performance at higher potential regions, it is very important to investigate its cyclic performance in the lower voltage region typically at 0–3 V to utilize it as a high performance electrode material for HSC application. In this work, we are the first to explore the possibility of employing LCPF as a cathode material for HSC application. In this connection, we prepared a well developed LCPF material using a solid state process and report the electrochemical capacitive behavior of a novel HSC consisting of LCPF and AC electrodes in 1 M $LiPF_6$ electrolyte solution at different current densities.

2 Experimental

LCPF powder was prepared using a two-step solid state method. At first, $LiCoPO_4$ powder was synthesized by a conventional solid state route. Stoichiometric amounts of $LiOH \cdot H_2O$ (Junsei, Japan), Co_3O_4 (Sigma-Aldrich, USA) and $(NH_4)_2HPO_4$ (Sigma-Aldrich, USA) were ground using a planetary ball mill for 3 h and pelletized. The pellets were heated at 400 °C for 10 h to eliminate hydroxyl and ammonia components. The final calcination was carried out at 800 °C for 10 h in air atmosphere to obtain $LiCoPO_4$. In order to get Li_2CoPO_4F, the obtained $LiCoPO_4$ powders were mixed with LiF (Wako, Japan), pelletized and then fired at 700 °C for 1.5 h under an Ar atmosphere and subsequently quenched to room temperature. The obtained LCPF was crushed into ultrafine powders and subjected to physical and electrochemical characterizations.

The structural property of LCPF powders was recorded using X-ray diffractometry (XRD, Rint 1000, Rigaku, Japan) with a Cu Kα radiation source. The surface morphology of the sample was analyzed using scanning electron microscopy (SEM, S-4700 microscope, Hitachi, Japan) and a transmission electron microscope (TEM, TecnaiF20, Philips, Holland). To evaluate the electrochemical behavior of each individual electrode, the electrochemical measurements were carried out using the half cells, in which either LCPF or AC acted as the working electrode with lithium foil as the counter electrode. The LCPF electrode was composed of 80% active material, 10% conductive additive (Ketjenblack), and 10% binder (Teflonized acetylene black). The mixture was pressed on a 200 mm^2 stainless steel mesh that served as the current collector at a pressure of 200 kg cm^{-2} and dried at 160 °C for 4 h in an oven. The same procedure was adopted for the preparation of the AC electrode. The half cells were fabricated using CR 2032 coin cell configuration in an argon filled glove box by pressing a working electrode, porous polypropylene separator (Celgard 3401) and lithium counter electrode with 1 M $LiPF_6$ in EC/DMC (1 : 1 v/v, Techno Semichem Co., Ltd, Korea) as the electrolyte solution. The HSC was assembled with the LCPF cathode and AC anode after optimizing the mass ratio of the active materials. For comparison, $LiCoPO_4$ (LCP)/AC and AC/AC cells were also fabricated using the above mentioned method. The cyclic voltammetry (CV) and the electrochemical impedance spectroscopy (EIS) studies were performed using an electrochemical analyzer (SP-150, Bio-Logic, France). The cycling studies of HSC were carried out between 0 and 3 V at different current densities using a cycle tester (WBCS 3000, Won-A-Tech, Korea) in galvanostatic mode. The effective series resistance (R_{ESR}), coulombic efficiency (CE) and the capacitance from the EIS studies were calculated using the formulae described elsewhere.[25–27] The specific energy (ED) and power (PD) densities for the cells were determined from charge–discharge studies as follows.[11,31]

$$PD = IV/2m \ (W\ kg^{-1})$$

$$ED = PD \times t/3600 \ (W\ h\ kg^{-1})$$

where m is the mass of active materials from both electrodes, I, the current applied, t, the discharge time and V being the cell voltage. The optimized total weight of active materials used, based on both cathode and anode, was 14 mg.

3 Result and discussion

Fig. 1a presents the XRD pattern of LCPF powder prepared at 700 °C for 1.5 h. It is being noted that very limited literature is available on the preparation of phase pure LCPF.[23,24] In our study, there is almost no impurities phase like Li_3PO_4, $LiCoPO_4$ and LiF observed within the recorded area, which suggested that highly crystalline and phase pure LCPF powders have been successfully synthesized. All diffraction peaks can be indexed based on the orthorhombic structure with *Pnma* space group[21]

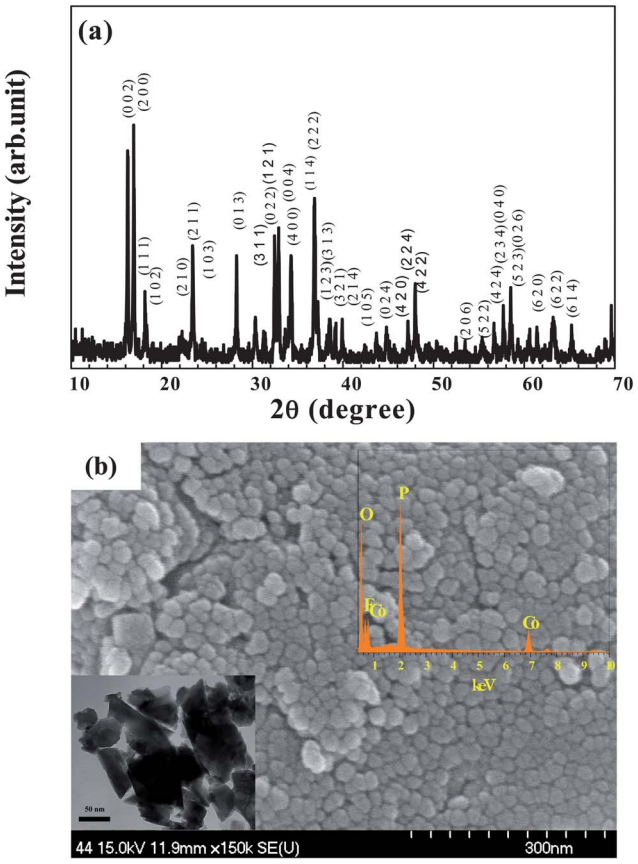

Fig. 1 (a) X-ray diffraction pattern and (b) SEM with EDAX and TEM image of Li_2CoPO_4F nanoparticles prepared using a two-step solid state method at 700 °C.

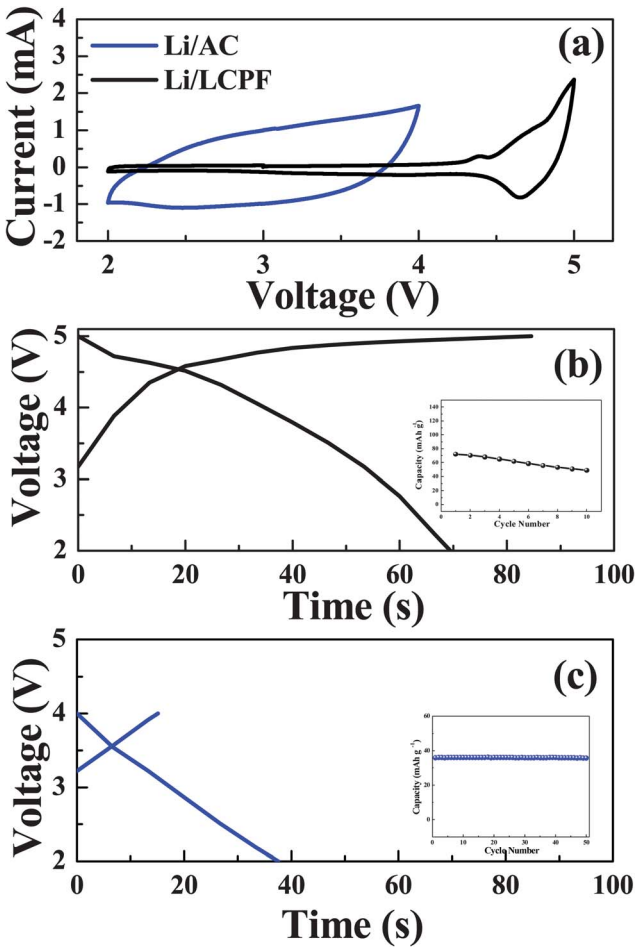

Fig. 2 (a) CV curves of Li/LCPF and Li/AC cells, C–D of (b) the Li/LCPF cell between 2 and 5 V and (c) the Li/AC cell between 2 and 4 V at the constant current density of 400 mA g^{-1} in 1 M $LiPF_6$ (1 : 1 EC/DMC) electrolyte. The corresponding cycle performance data are given as insets.

(JCPDS card no.: 56-1493). The calculated cell parameters were about $a = 10.462$ Å, $b = 6.373$ Å and $c = 10.892$ Å, which closely agreed with previous reports.[21–24] It is evident from SEM and TEM images in Fig. 1b that the LCPF powders consist of well developed particles with a narrow size distribution. From the images, the average particle size of about 50–100 nm was estimated. It is well known that lithium insertion/extraction is much easier in polycrystalline materials with a mean size of around 100 nm and could be enhanced due to the reduction of diffusion pathways for Li^+ ions, which also guided the faster electronic transport through its size effect. The surface of the particles remains smooth even after quenching from high temperature. Partial aggregation of the small sized particles can also be seen in the SEM of LCPF in Fig. 1b. Energy dispersive X-ray spectroscopy (EDS) of LCPF was also conducted and is presented in the inset of Fig. 1b. The EDS clearly revealed that the LCPF powders are composed of Co, F, P, and O species; Li cannot be detected in EDS because of its low energy density. The P/F ratio was found to be 0.17 : 0.16 from EDS results, which is in good agreement with the stoichiometric ratio of P/F = 1, which is the same as that of the Co/F ratio.

The electrochemical behavior of the individual electrodes (LCPF or AC) was investigated using CV studies versus the lithium electrode. The CV curves were recorded for LCPF and AC electrodes respectively at the scan rate of 0.5 mV s^{-1} and 5 mV s^{-1} and corresponding traces are shown in Fig. 2a. It is obvious from Fig. 2a that the CVs of two materials have shown different electrochemical behaviors. The LCPF electrode exhibited redox behaviors at ~4.4 V and ~4.8 V during the positive sweep and at ~4.65 V during the negative sweep between the voltage range of 2 and 5 V whereas AC showed a typical double layer capacitive behavior (*i.e.* rectangular shape) between 2 and 4 V.

The first C–D profiles of individual electrodes *vs.* the Li electrode at the constant current density of 400 mA g^{-1} in 1 M $LiPF_6$ electrolyte solution are illustrated in Fig. 2b and c. In order to avoid the gas evolution and electrolyte depletion, the cutoff potentials for LCPF and AC were set at 2–5 V and 2–4 V, respectively. It can be seen from Fig. 2b and c that the LCPF electrode exhibited a typical lithium intercalation/deintercalation property while the AC electrode showed a typical capacitor profile along with the absorption and desorption of PF_6^- anion on the surface of the AC electrode.[26] The corresponding discharge capacity of about 70 and 36 mA h g^{-1} was obtained respectively for LCPF and AC electrodes. It is obvious that the applied voltage equally divides between the electrodes in symmetrical supercapacitors with the same mass of the active materials at each electrode whereas this is not the case in HSCs

fabricated with different cathode and anode materials with different storage mechanisms. The applied voltage will split based on the capacitive performance of each electrode. Since the capacitance of each electrode in a HSC is directly related to its weight, a mass balance is required to obtain the optimum cell voltage and high energy density.[11] In this connection, the electrode mass ratio for HSC fabrication was obtained from the electrochemical performance of the LCPF and AC electrode against the lithium counter electrode. Hence, the mass ratio of LCPF to AC in the HSC was fixed at 2 : 1.[11,25] During the initial charging, the LCPF and AC electrodes got polarized in the positive and negative direction and started acting as the cathode and anode in the HSC cell configuration, respectively.

Fig. 3a illustrates the CV studies of the LCPF/AC cell between 0 and 3 V at different scan rates. All CV curves were almost rectangular in shape and exhibited a near mirror-image current response on voltage reversal at each end potential. This clearly indicates that the LCPF/AC cell has capacitive behavior within the potential range of 0–3 V. The shapes of CV curves for the LCPF/AC cell revealed that the capacitive characteristic is distinct from that of the electric double-layer capacitor, which could be attributed to the overlapping effect of two different energy storage mechanisms.[15,25] Unlike the AC anode, where energy storage arises from the charge separation at the electrode–electrolyte interface, the LCPF cathode stores energy by utilizing Faradaic electron transfer reaction and reversible phase transformation. A similar trend in the deviation of CV curves from the rectangular shapes was also reported by Wang *et al.* for the CNT/TiO_2 cell in a non-aqueous electrolyte.[5,28] Furthermore, the CV curves of the LCPF/AC cell did not have shape changes even at higher scan rates, revealing that the hybrid cell is highly stable in 1 M $LiPF_6$ electrolyte within the observed potential range. The capacitance of the LCPF/AC cell calculated from the CV studies was about 41, 36, 32, 27, 22 and 20 F g^{-1} at 2, 3, 5, 7, 10 and 15 mV s^{-1} scan rates, respectively. It could be noted that the specific capacitance gets decreased with increasing scan rate, which is attributed to the reduced diffusion rate of the Li^+ ions in the pores as well as due to the surface adsorption process.[26,27] At higher scan rates, the electrochemical storage process takes place mainly at the surface of the electroactive material than at the bulk. This reduced the penetration of Li^+ into the bulk, thereby reducing the diffusion rate of Li^+ ions. Hence, only the surface of the material actively participated in the electrochemical reaction at higher scan rates. The overall reduction in surface area for electrochemical reaction during high scan rates decreased the specific capacitance of the LCPF/AC cell.

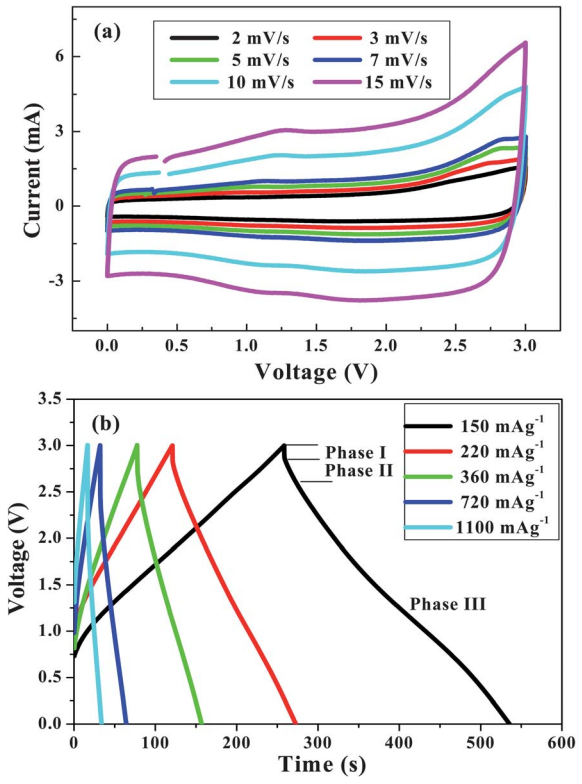

Fig. 3 (a) CV curves of the LCPF/AC cell at different scan rates and (b) C–D profiles of the HSC between 0 and 3 V at different current densities from 150 to 1100 mA g^{-1}.

The C–D studies of the HSC cell were conducted between 0 and 3 V at different current densities ranging from 150 to 1100 mA g^{-1} and the corresponding C–D curves are presented in Fig. 3b. Although an almost linear variation of cell voltage is observed during the charge and discharge process, the curve is not as well-shaped triangles as an ideal capacitive behavior should be. This may be due to the combination of two different kinds of mechanism involved in the energy storage process. As seen from Fig. 3b, the C–D curves consist of a small voltage drop *i.e.* R_{ESR} arises from the internal resistance (phase I), a double layer capacitive region due to ion separation at the electrode–electrolyte interface (phase II) and a Faradaic component attributed to the charge-transfer reaction of the LCPF material in the longer time region (phase III). This clearly demonstrated that the LCPF/AC cell exhibited characteristics of both battery and EDLC types.[10,25,28] Moreover, the magnitude of the R_{ESR} drop increased with increasing current density. The energy storage mechanism at the AC anode is based on the formation of an electrical double layer from a non-Faradaic process together with the PF_6^- anion present in the electrolyte,[26] whereas the LCPF cathode takes advantage of electron transfer that resulted from the Li^+ insertion process to produce pseudocapacitance behavior. The possible reaction mechanism of a LCPF based HSC could be written as follows:

$$Li_2Co^{2+}PO_4F \leftrightarrow Li_{2-x}Co^{3+}PO_4F + xLi^+ + xe^- \quad (1)$$

$$AC + xe^- \leftrightarrow AC\,(xe^-) + //xPF_6^- \text{ (// stands for double layer)} \quad (2)$$

During the charging process, Li^+ ions are released from the LCPF structure into the electrolyte and then trapped into the LCPF electrode from the electrolyte solution during the discharge process, which ensures the high energy density of the HSC.[5] In the mean time, PF_6^- anions also get adsorbed and desorbed on the surface of the AC electrode to produce the double layer during the C–D process, providing the essential power density. The cell discharge capacitance (C_{cell}) and the

specific discharge capacitance (C_{dc}) were calculated using the formulae $C_{cell} = (it/\Delta V)$ and $C_{dc} = (4C_{cell}/m)$, respectively, where i is the current density (mA), t is the discharge time (s), ΔV is the potential difference (V) and m is the total mass of the electroactive materials used in both electrodes.[25,27] The C_{dc} values calculated from the C–D studies were about 42, 34, 30, 24 and 21 F g^{-1} at a current density of 150, 220, 360, 720 and 1100 mA g^{-1}, respectively. The C-rate was also calculated based on the theoretical capacity of LCPF for one lithium intercalation reaction. Accordingly, 1 C equals 143 mA g^{-1} and hence, the calculated C-rates corresponding to the above currents were approximately 1.05 C, 1.5 C, 2.5 C, 5 C and 8 C, respectively. It is obvious that the capacitance decreases with increasing scan rates due to low utilization of active materials at high current rates. At high current, Li^+ intercalation into the bulk of LCPF and interfacial Li^+ storage on the surface will be limited, because the ions could approach only the outer surface of the electrode material.[9,26] The specific current dependence of average R_{ESR}, ED and PD of the LCPF/AC cell was also calculated from the C–D studies and summarized in Fig. 4. Fig. 4a clearly shows that the LCPF/AC cell exhibited low resistance even at high current densities. It can also be seen from Fig. 4b that the LCPF/AC cell delivered an ED value of about 47 W h kg^{-1} at a PD of 215 W kg^{-1} (based on the total weight of the active materials used in both electrodes) and still maintaining the ED value of 24 W h kg^{-1} even at a high PD of 1607 W kg^{-1}. It is worth mentioning here that LCPF is capable of delivering twice the capacitance and specific energy due to its strong ionicity of M–F bonds than that of $LiCoPO_4$.[20]

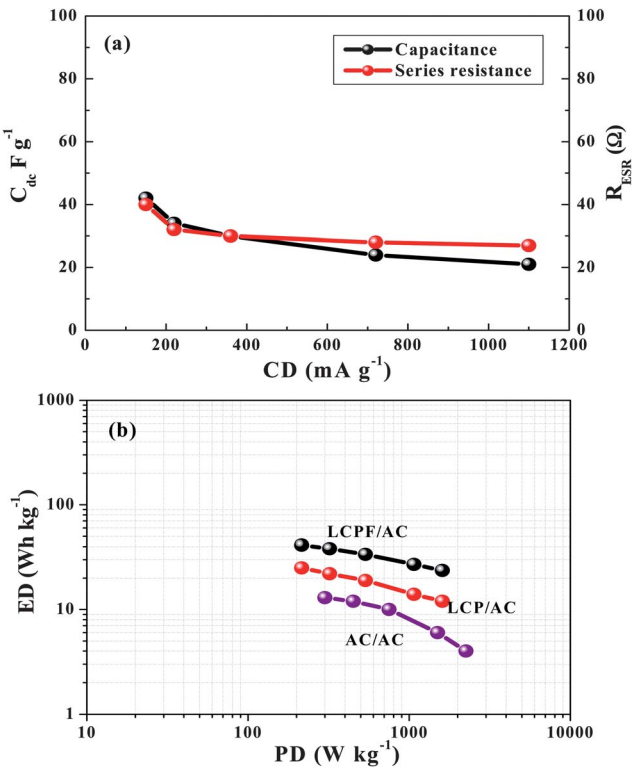

Fig. 4 (a) Specific current dependence of series resistance and discharge capacitance of the LCPF/AC cell at different current densities and (b) Ragone plot of power density *versus* energy density for LCPF/AC and AC/AC cells.

In this work, we almost achieved as twice as the capacitance and enhanced energy and power densities than $LiCoPO_4$ based HSCs (LCP/AC) as shown in Fig. S2, S3† and 4b and the one reported by Vasanthi *et al.* for $LiCoPO_4$/CNF (carbon nano foam) systems.[15] Furthermore, the ED obtained in the present work (24 W h kg^{-1}) is higher than that of any commercialized capacitors typically 15 W h kg^{-1} for AC/$Ni(OH)_2$, 20 W h Kg^{-1} for AC/$Li_4Ti_5O_{12}$ and also larger than that of the AC/AC system (4 W h kg^{-1}) as shown in Fig. 5b and S4.† It can also be competitive with lead–acid battery technology but with enhanced PD, excellent rate performance along with prolonged cycle life.

In order to find out the rate performance, the LCPF/AC cell was charged and discharged for 1000 times at each current density and the observed cycling behavior is presented in Fig. 5. The data illustrated that the LCPF/AC cell showed excellent capacitance retention even at high current densities. The LCPF/AC cell delivered an initial discharge capacitance of 42, 34, 30, 24 and 21 F g^{-1} and maintained about 37, 32, 29, 24 and 21 F g^{-1} at a current density of 150, 220, 360, 720 and 1100 mA g^{-1}, respectively, corresponding to the retention of 88, 94, 97, 100 and 100% after 1000 cycles. N. R. Khasanova *et al.* reported that the Li_2CoPO_4F material was found to undergo structural relaxation during charge–discharge that resulted in the formation of a modified framework structure. The initial cycles are used for fine tuning of the structure and hence, it was believed to have an effect on the cycle performance of the LCPF/AC cell at low current densities.[23] A similar effect can be expected in the present case. As the number of cycles increases, the stable structure formed during initial cycles helped in retaining high reversibility of lithium even at high current rates because of the increase in interstitial space created during modified framework formation and volume expansion occurred thereby. The increasing behavior of capacity retention even at a high current density resulted from its low internal resistance and high crystallinity of LCPF, since both of these properties facilitate better Li-ion diffusion.[29] It is noteworthy that decreasing the internal resistance directly increases the current flow on the surface of electrodes, ensuring more lithium ion diffusion

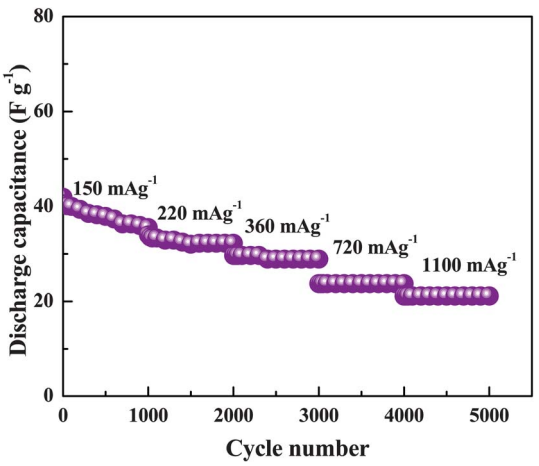

Fig. 5 Rate performance of the LCPF/AC cell at different current densities from 150 to 1100 mA g^{-1} for 1000 cycles each.

towards the electrode, thereby remarkably enhancing the cycling behavior even at high current rates.[26] On the other hand, highly crystalline small sized particles reduced the diffusion pathway for lithium ion migration, which significantly improved the contact between active sites thus enhancing the ionic transport at high current rates, and hence the cycling performance was improved.[29,30] In addition, the stable cycling behavior at high current rates was also attributed to the careful optimization of the counter electrode. It was also reported that the appropriate optimization of electrode materials is essential for achieving enhanced cycling performance at high current rates.[11]

Since long term cycling of the HSC at high current is an essential feature for adopting in high power applications, the stability of the LCPF/AC cell was evaluated by examination of 30 000 cycles at a constant current density of 1100 mA g^{-1} and the results are presented in Fig. 6. As seen from Fig. 6a, the discharge time difference between 1st and 30 000th C–D curves was very small, demonstrating its excellent electrochemical stability. Moreover, the cell also exhibited a high coulombic efficiency close to 100%. Furthermore, as shown in Fig. 6b, the LCPF/AC cell not only delivered an energy density of ~24 W h kg^{-1} at 1100 mA g^{-1}, but also maintained excellent stability until 30 000 deep C–D cycles. The ED initially dropped by *ca.* 5% from 23.6 to 22.5 W h kg^{-1} during the first 10 000 cycles and then remained almost constant thereafter until 30 000 cycles. To the best of our knowledge, it is the best cycling performance for HSCs containing a lithium intercalation electrode than any other hybrid devices reported in an organic electrolyte.[10–17,25,26,32–35] Obviously, the excellent cycling behavior of the LCPF cathode utilized in the HSC complements the intrinsic cycling stability of the AC electrode as well as the low internal resistance of the cell as shown in Fig. 4a. The observed S_{ED} and S_{PD} values for the LCPF/AC cell outperformed other hybrid cells with lithium intercalating components. For comparison, Wang *et al.* reported the $LiMn_2O_4$/AC cell with the S_{ED} and S_{PD} of 35 W h kg^{-1} and 125 W kg^{-1}, respectively.[12] Aravindan *et al.* showed the $LiTi_2(PO_4)_3$/AC cell performance with S_{ED} of 14 W h kg^{-1} and S_{PD} of 180 W kg^{-1}.[31] The hybrid cell consisting of $LiTi_2(PO_4)_3$ and MnO_2 electrodes exhibited the S_{ED} and S_{PD} of 43 W h kg^{-1} and 200 W kg^{-1}, respectively.[32] A hybrid cell with $Li_4Ti_5O_{12}$/poly(methyl)thiophene configuration has an S_{ED} of 10 W h kg^{-1} and an S_{PD} of 30 W h kg^{-1}.[33] Also, the performance of the LCPF/AC cell is higher than the hybrid cell which consists of AC/nanocrystalline-$Li_4Ti_5O_{12}$ attached on carbon nanofibres with 1 M $LiPF_6$ in the EC/EMC/DMC (1 : 1 : 1 vol) electrolyte.[34]

EIS studies were conducted within the frequency range of 100 kHz to 100 mHz at open circuit voltage. The Nyquist plot of the LCPF/AC cell shown in Fig. 7 includes a semicircle at high-frequency intercept of the real axis, followed by a straight line at the low frequency region. The straight line with a slope corresponds to the diffusion control process and the semicircle part at the high frequency region is related to reaction kinetics at the electrode and electrolyte interface and is also known as charge transfer resistance (R_{ct}). The specific capacitance of the LCPF/AC cell for AC impedance studies was calculated to be about 38 F g^{-1}. The slight variation in the capacitance from the one calculated from C–D may be attributed to the penetration of alternative current through the electrode surface into the bulk with more hindrance.[35] Good fitting data were obtained for the LCPF/AC cell by using an equivalent circuit as shown in the inset of Fig. 6. As illustrated in Fig. 6, there was a small difference in R_{ct} observed for the cell cycled before and after 1000 C–D cycles, whereas the Nyquist plots of the cell recorded after 1000 and 30 000 cycles were almost identical, which supports the

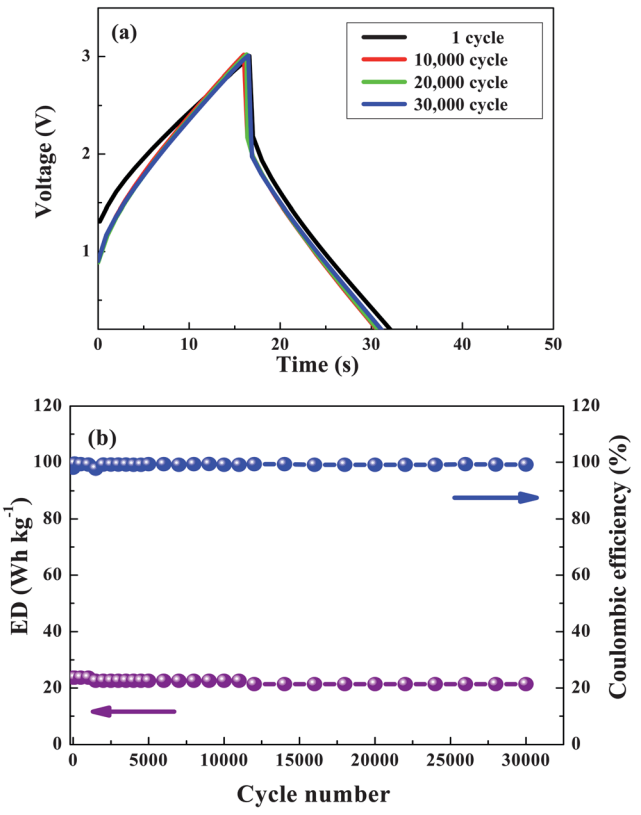

Fig. 6 (a) 1st, 10 000th, 20 000th and 30 000th charge–discharge curves of the LCPF/AC cell recorded at 1100 mA g^{-1} current between 0 and 3 V and (b) variation of ED (W h kg^{-1}) with the number of cycles for the LCPF/AC cell.

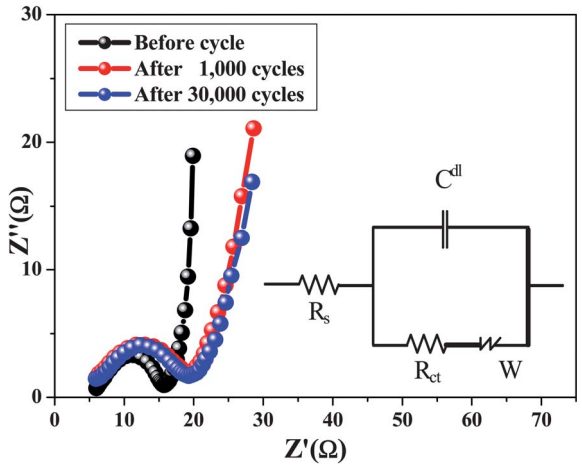

Fig. 7 Nyquist plot of the LCPF/AC cell recorded before and after 1000 and 30 000 cycles. The equivalent circuit is given in the inset.

result of cycling test, indicating that the LCPF/AC cell has a good capacitive performance between 0 and 3 V even at high current rates.

The structural stability of cathode after cycling was examined through SEM analysis and results are presented in Fig. S5.† After cycling, the cathodes were carefully removed from the coin cell inside the glove box, and then washed with DMC followed by drying at 160 °C for 12 h. As can be seen from Fig. S5,† no obvious structural changes were observed even after severe cycling when compared with the particles before cycling, as illustrated in Fig. 1b. This clearly revealed the high structural stability of LCPF and hence enhanced the electrochemical performance with prolonged cycling under harsh conditions.

4 Conclusion

A novel approach has been made to fabricate a hybrid capacitor consisting of Li_2CoPO_4F as the cathode and activated carbon as the anode in an organic electrolyte. The results obtained in charge–discharge studies clearly demonstrated that the LCPF/AC cell exhibited capacitive performance between the voltage range of 0 and 3 V with high cycle stability and low internal resistance even at high current densities. Furthermore, the maximum specific capacitance of about 42 F g^{-1} and an energy density of 47 W h kg^{-1} were obtained at a current density of 150 mA g^{-1}. The LCPF/AC cell also exhibited a power density of 1607 W kg^{-1} as well as a specific energy of ~24 W h kg^{-1} at a high current density of 1100 mA g^{-1} with more than 92% retention of its initial value after 30 000 C–D cycles. Considering the above results, we suggest that the Li_2CoPO_4F material could be a prospective candidate for a cathode in high rate hybrid capacitor applications.

Acknowledgements

This work was supported by the National Research Foundation of Korea Grant funded by the Korean Government (MEST) (NRF-2011-C1AAA001-0030538).

References

1 B. E. Conway, *J. Electrochem. Soc.*, 1991, **138**, 1539–1548.
2 E. Frackowiak, *Phys. Chem. Chem. Phys.*, 2007, **9**, 1774–1785.
3 G. Wang, L. Zhang and J. Zhang, *Chem. Soc. Rev.*, 2012, **41**, 797–828.
4 G. A. Snook, P. Kao and A. S. Best, *J. Power Sources*, 2011, **196**(1), 1.
5 G. G. Amatucci, F. Badway, A. D. Pasquier and T. Zheng, *J. Electrochem. Soc.*, 2001, **148**, A930–A939.
6 J. Y. Luo and Y. Y. Xia, *J. Power Sources*, 2009, **186**, 224–227.
7 Y. Xue, Y. Chen, M. L. Zhang and Y. D. Yan, *Mater. Lett.*, 2008, **62**, 3884–3886.
8 N. W. Duffy, W. Baldsing and A. G. Pandolfo, *Electrochim. Acta*, 2008, **54**, 535–539.
9 N. Yu and L. Gao, *Electrochem. Commun.*, 2009, **11**, 220–222.
10 A. D. Pasquier, A. Laforgue and P. Simon, *J. Power Sources*, 2004, **125**, 95–102.
11 V. Aravindan, W. Chuiling and S. Madhavi, *J. Mater. Chem.*, 2012, **22**, 16026–16031.
12 Y. G. Wang and Y. Xia, *Electrochem. Commun.*, 2005, **7**, 1138–1142.
13 Y. J. Hao, Q. Y. Lai, X. Y. Xu and L. Wang, *Mater. Chem. Phys.*, 2011, **126**, 432–436.
14 Y. G. Wang, J. Y. Luo, C. X. Wang and Y. Y. Xia, *J. Electrochem. Soc.*, 2006, **153**, A1425–A1431.
15 R. Vasanthi, D. Kalpana and N. G. Renganathan, *J. Solid State Electrochem.*, 2007, **12**, 961–969.
16 H. Wu, C. V. Rao and B. Rambabu, *Mater. Chem. Phys.*, 2009, **116**, 532–535.
17 J. Barker, M. Y. Saidi, R. K. B. Gover, P. Burns and A. Bryan, *J. Power Sources*, 2007, **174**, 927–931.
18 T. N. Ramesh, K. T. Lee, B. L. Ellis and L. F. Nazar, *Electrochem. Solid-State Lett.*, 2010, **13**, A43–A47.
19 M. Dutreilh, C. Chevalier, M. E. Ghozzi, D. Avignant and J. M. Montel, *J. Solid State Chem.*, 1999, **142**, 1–5.
20 N. Recham, J. N. Chotard, J. C. Jumas, L. Laffont, M. Armand and J. M. Tarascon, *Chem. Mater.*, 2010, **22**, 1142–1148.
21 S. Okada, M. Ueno, Y. Uebou and J. Yamaki, *J. Power Sources*, 2005, **146**, 565–569.
22 E. D. Botto, C. Bourbon, S. Patoux, P. Rozier and M. Dolle, *J. Power Sources*, 2011, **196**, 2274–2278.
23 N. R. Khasanova, A. N. Gavrilov, E. V. Antipov, K. G. Bramnik and H. Hibst, *J. Power Sources*, 2011, **196**, 355–360.
24 D. Wang, J. Xiao, W. Xu, Z. Nie, C. Wang, G. Graff and J. G. Zhang, *J. Power Sources*, 2011, **196**, 2241–2245.
25 K. Karthikeyan, V. Aravindan, S. B. Lee, I. C. Jang, H. H. Lim, G. J. Park, M. Yoshio and Y. S. Lee, *J. Power Sources*, 2010, **195**, 3761–3764.
26 K. Karthikeyan, V. Aravindan, S. B. Lee, I. C. Jang, H. H. Lim, G. J. Park, M. Yoshio and Y. S. Lee, *J. Alloys Compd.*, 2010, **504**, 224–227.
27 Y. Zhu, S. Murali, M. D. Stoller, K. J. Ganesh, W. Cai, P. J. Ferreira, A. Pirkle, R. M. Wallace, K. A. Cychosz, M. Thommes, D. Su, E. A. Stach and R. S. Ruoff, *Science*, 2011, **332**, 1537–1541.
28 Q. Wang, Z. Wen and J. Li, *Adv. Funct. Mater.*, 2006, **16**, 2141–2146.
29 K. Karthikeyan, S. Amaresh, V. Aravindan, H. Kim, K. S. Kang and Y. S. Lee, *J. Mater. Chem. A*, 2013, **1**, 707–714.
30 Z. Wang, Y. Sun, L. Chen and X. Huang, *J. Electrochem. Soc.*, 2004, **151**, A914–A921.
31 V. Aravindan, W. Chuiling, M. V. Reddy, G. V. S. Rao, B. V. R. Chowdari and S. Madhavi, *Phys. Chem. Chem. Phys.*, 2012, **14**, 5808–5814.
32 J. Y. Luo, J. L. Liu, P. He and Y. Y. Xia, *Electrochim. Acta*, 2008, **53**, 8128–8133.
33 A. D. Pasquier, A. Laforgue and P. Simon, *J. Power Sources*, 2004, **125**, 95–102.
34 K. Naoi, S. Ishimoto, Y. Isobe and S. Aoyagi, *J. Power Sources*, 2010, **195**, 6250–6254.
35 W. Xing, S. Z. Qiao, R. G. Ding, F. Li, G. Q. Lu, Z. F. Yan and H. M. Cheng, *Carbon*, 2006, **44**, 216–224.

